Molecular Mechanism of the Electron Transfer Reaction in Cytochrome $P450_{cam}$−Putidaredoxin: Roles of Glutamine 360 at the Heme Proximal Site†

Takehiko Tosha,‡ Shiro Yoshioka,‡ Hiroshi Hori,§ Satoshi Takahashi,‡ Koichiro Ishimori,*,‡ and Isao Morishima*,‡

Department of Molecular Engineering, Graduate School of Engineering, Kyoto University, Kyoto 606-8501, Japan, and Division of Biophysical Engineering, Graduate School of Engineering Science, Osaka University, Osaka 560-8531, Japan

Received May 9, 2002; Revised Manuscript Received August 29, 2002

ABSTRACT: We characterized electron transfer (ET) from putidaredoxin (Pdx) to the mutants of cytochrome $P450_{cam}$ ($P450_{cam}$), in which one of the residues located on the putative binding site to Pdx, Gln360, was replaced with Glu, Lys, and Leu. The kinetic analysis of the ET reactions from reduced Pdx to ferric $P450_{cam}$ (the first ET) and to ferrous oxygenated $P450_{cam}$ (the second ET) showed the dissociation constants (K_m) that were moderately perturbed for the Lys and Leu mutants and the distinctly increased for the Glu mutant. Although the alterations in K_m indicate that Gln360 is located at the Pdx binding site, the effects of the Gln360 mutations (0.66−20-fold of that of wild type) are smaller than those of the Arg112 mutants (25−2500-fold of that of wild type) [Unno, M., et al. (1996) *J. Biol. Chem. 271*, 17869−17874], allowing us to conclude that Gln360 much less contributes to the complexation with Pdx than Arg112. The first ET rate (35 s^{-1} for wild-type $P450_{cam}$) was substantially reduced in the Glu mutant (5.4 s^{-1}), while less perturbation was observed for the Lys (53 s^{-1}) and Leu (23 s^{-1}) mutants. In the second ET reaction, the retarded ET rate was detected only in the Glu mutant but not in the Lys and Leu mutants. These results showed the smaller mutational effects of Gln360 on the ET reactions than those of the Arg112 mutants. In contrast to the moderate perturbations in the kinetic parameters, the mutations at Gln360 significantly affected both the standard enthalpy and entropy of the redox reaction of $P450_{cam}$, which cause the negative shift of the redox potentials for the Fe^{3+}/Fe^{2+} couple by 20−70 mV. Since the amide group of Gln360 is located near the carbonyl oxygen of the amide group of the axial cysteine, it is plausible that the mutation at Gln360 perturbs the electronic interaction of the axial ligand with heme iron, resulting in the reduction of the redox potentials. We, therefore, conclude that Gln360 primarily regulates the ET reaction of $P450_{cam}$ by modulating the redox potential of the heme iron and not by the specific interaction with Pdx or the formation of the ET pathway that are proposed as the regulation mechanism of Arg112.

Cytochrome P450 (P450) is a family of heme-containing monooxygenases that metabolize a wide variety of natural and unnatural substances such as steroids, fatty acids, hydrocarbons, and xenobiotics (*1*). The reaction cycle of monooxygenation catalyzed by P450 is depicted in Figure 1, showing the requirement of two distinct ET[1] processes in the single turnover. In the first ET process, the resting state of P450, of which heme iron is in the ferric state, accepts one electron from the redox partner to produce the ferrous form of P450. After the binding of a molecular oxygen to the ferrous heme iron to form oxygenated P450, the second electron is transferred to activate the O−O bond and to initiate the oxygen transfer to the substrate. The ET reactions between P450 and the redox partner, therefore, are essential for the catalytic cycle of P450. Accordingly, a number of studies have been conducted to elucidate the molecular mechanism of the ET reactions for more than 30 years.

The most interesting aspect of the ET reactions between P450 and the redox partner is the selectivity for the specific redox partner. Several studies on the cross-reactivities of P450s with various redox partners revealed that the nonphysiological partners are less efficient than the physiological partner in the ET reactions and in the enzymatic activities (*2*−*4*). For example, Lehnerer et al. reported that adrenodoxin, the redox partner for the mitochondrial P450s, can donate electrons to the microsomal P450 2B4 with 73% of the uncoupling reaction (H_2O_2 production/NADPH oxidation), which is much higher than that of the physiological P450 reductase system (25% of the uncoupling reaction) (*3*). Jenkins and Waterman showed that flavodoxin and NADPH−flavodoxin reductase can serve as an electron transfer system for microsomal P450c17 instead of the physiological redox partner. The progesterone 17α-hydroxylase activity of P450c17 with flavodoxin and NADPH−flavodoxin reductase was suppressed to 14% of that supported by the physiological partner, P450 reductase (*4*). These results imply that P450 and the redox partner form a specific complex to effectively transfer the electrons.

† This work is supported by grants-in-aid for scientific research on priority areas Molecular Biometalics (08249102 to I.M.) from the Ministry of Education, Science, Culture, and Sports.

* To whom correspondence should be addressed. Tel: +81-75-753-5945. Fax: +81-75-751-7611. E-mail: morisima@mds.moleng.kyoto-u.ac.jp (I.M.) or koichiro@mds.moleng.kyoto-u.ac.jp (K.I.).

‡ Kyoto University.

§ Osaka University.

[1] Abbreviations: $P450_{cam}$, cytochrome P450 CYP101 isolated from *Pseudomonas putida*; Pdx, putidaredoxin; PdR, NADH−putidaredoxin reductase; ET, electron transfer.

10.1021/bi0261037 CCC: $22.00
Published on Web 11/01/2002

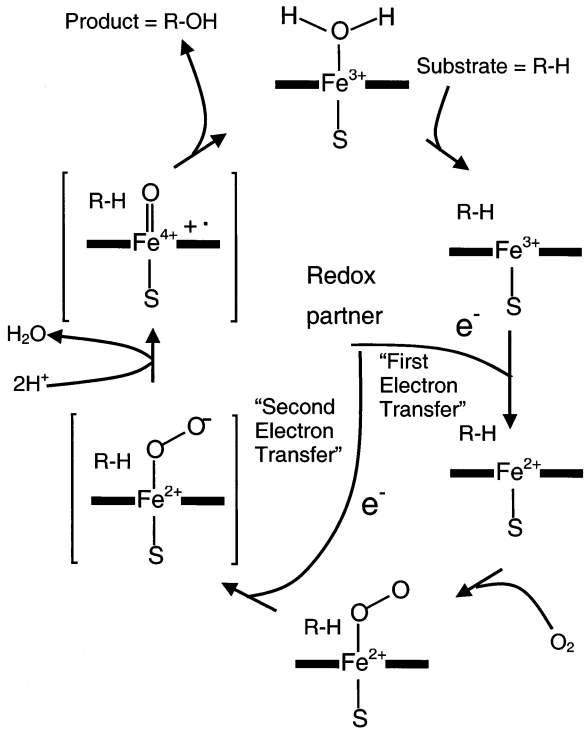

FIGURE 1: Proposed reaction cycle of cytochrome P450. S is the axial thiolate ligand, and the thick line is the porphyrin ring of the heme. The compounds depicted in brackets are proposed structures of putative reaction intermediates.

Despite the accumulation of an impressive body of knowledge on the ET reactions, the structural factors regulating the ET reaction, namely, the specific recognition between P450 and the redox partner, have poorly been understood. The situation is primarily caused by the absence of the three-dimensional structures for the ET complex between P450 and the redox partner. In fact, a bacterial cytochrome P450 from *Pseudomonas putida* (CYP101), $P450_{cam}$, and an iron−sulfur [2Fe-2S] protein, putidaredoxin (Pdx), are the unique redox pair, with each three-dimensional structure now available at the atomic level (*5*, *6*). Many researchers, therefore, have investigated the ET mechanism between $P450_{cam}$ and Pdx to understand the structure−function relationship of P450 and its redox partner in detail.

$P450_{cam}$ catalyzes the conversion of *d*-camphor to 5-*exo*-hydroxycamphor by utilizing two reducing equivalents and a molecular oxygen (*7*). Two electrons from NADH are transferred via NADH−putidaredoxin reductase (PdR), a flavoprotein, to Pdx and finally to the heme iron of $P450_{cam}$. The selectivity in the ET reactions is also observed in the $P450_{cam}$−Pdx pair. For example, adrenodoxin is highly homologous to Pdx and has lower redox potential than Pdx but can donate only the first electron to $P450_{cam}$, not the second electron (*8*). The preferential ET from Pdx to $P450_{cam}$ is supposed to be derived from the specific interactions of Pdx with $P450_{cam}$, and the identification of the amino acid residues responsible for the specific binding of Pdx with $P450_{cam}$ is, therefore, a keystone for the understanding of the ET process from Pdx to $P450_{cam}$.

To investigate the specific interactions between Pdx and $P450_{cam}$, several lines of mutagenetic and theoretical studies on the ET reaction between Pdx and $P450_{cam}$ have been carried out (*9*−*15*). The computer modeling of $P450_{cam}$ and cytochrome b_5 suggests that four basic amino acid residues on the $P450_{cam}$ surface near the axial ligand, Arg72, Arg112, Lys344, and Arg364 (*9*), are involved in the interface between $P450_{cam}$ and cytochrome b_5. The same residues are suggested to be similarly important for the interaction with Pdx. Actually the mutation of Arg112 evoked a drastic decrease in the catalytic activity of $P450_{cam}$ in the presence of Pdx (*10*) and demonstrated that Arg112 is located at the Pdx binding site. On the basis of these mutational studies, Pochapsky et al. proposed the model structure of the $P450_{cam}$−Pdx complex, which assumes a salt bridge between Arg112 and Asp38 in Pdx (*16*). The theoretical analysis of the ET pathway in the proposed $P450_{cam}$−Pdx complex indicates that Arg112 is also involved in the coupling between the 2Fe-2S cluster in Pdx and the heme iron of $P450_{cam}$ (*17*), which is consistent with the mutational study at Arg112. These modeling and mutational studies support the crucial roles of Arg112 in the specific binding to Pdx (*16*, *17*).

Although it is clear that Arg112 is vital to the specific interaction in the ET reaction of the $P450_{cam}$−Pdx system, some other interactions are suggested in the structural modeling of the $P450_{cam}$−Pdx complex (*16*). We noticed that there is an interprotein hydrogen bond between Gln360 of $P450_{cam}$ and Cys39 of Pdx in the model complex structure and hypothesized that Gln360 is also crucial for the ET reaction on the basis of the following observation. Gln360 is located at the interface of the putative Pdx binding site in $P450_{cam}$ and also hydrogen bonded to the axial ligand of $P450_{cam}$, as illustrated in Figure 2. We recently suggested that the hydrogen bond between Gln360 and the axial Cys (Cys357) controls the redox potential of $P450_{cam}$ (*18*). Furthermore, there is a possibility that the hydrogen bond between Gln360 and Cys39 might be the ET pathway, because the hydrogen bond is located almost along the vector connecting the axial Cys of $P450_{cam}$ and the iron−sulfur cluster of Pdx. It is thus likely that Gln360 possesses significant roles in the ET reaction between $P450_{cam}$ and Pdx such as the specific recognition of Pdx, the regulation of the redox potential, and the formation of the effective ET pathway.

In this paper, to examine the functional roles of Gln360 in the ET reactions between Pdx and $P450_{cam}$, we prepared three Gln360 mutants to perturb the hydrogen bonds with Pdx and the axial ligand of $P450_{cam}$. One of the mutations is Gln → Glu (Q360E), in which the amide group is replaced by the carboxyl group and the hydrogen bond to Cys39 in Pdx would be disrupted. The mutation to Leu (Q360L) would also disrupt the hydrogen bond, and the high hydrophobicity of the side chain might induce repulsive interactions with the carbonyl group of Cys39. Another mutant, the Q360K mutant, has a positively charged Lys residue at position 360, whose hydrogen bond to Cys39 in Pdx might be maintained due to the positive charge of the amino group. The ET properties of these mutants were characterized by measuring the ET rates for the first and second ET processes and the redox potentials to clarify the functional significance of Gln360 for the ET reactions.

MATERIALS AND METHODS

Sample Preparation. Site-directed mutagenesis was carried out by the method of Kunkel (*19*) using an M13mp19 phage vector containing the $P450_{cam}$ gene as a template (*20*). To

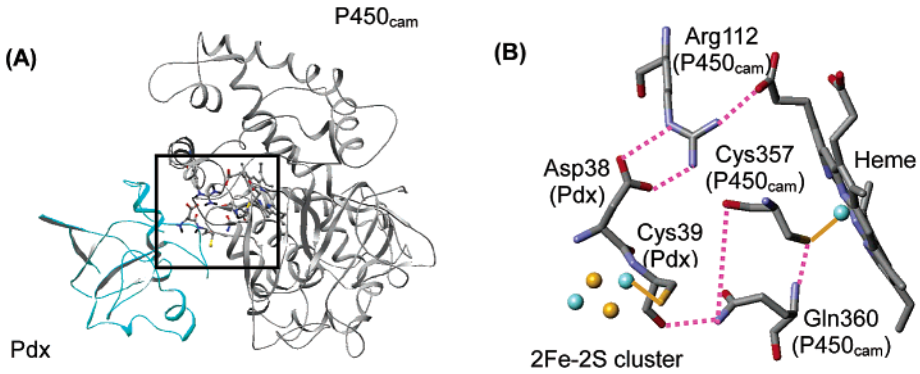

FIGURE 2: Putative structure of the $P450_{cam}$−Pdx complex proposed by Pochapsky et al. (*16*). Panel A shows the whole structure of the $P450_{cam}$−Pdx complex. The regions colored by gray and light blue correspond to $P450_{cam}$ and Pdx, respectively. Panel B represents the interface between $P450_{cam}$ and Pdx. The dotted lines indicate the presumed hydrogen bonds.

construct the expression vectors of the Gln360 mutants, the M13mp19 phage vector was digested by the restriction enzymes *Hin*dIII and *Eco*RV, and the fragments were ligated into T7 expression vectors (*20*, *21*). DNA sequencing was performed by the dye deoxy terminator method using an ABI 373A DNA sequencer (Applied Biosystems). Wild-type $P450_{cam}$ and its mutants were expressed in *Escherichia coli* strain BL21 as the apoenzymes in the inclusion body (*20*, *21*). The heme reconstitution and the purification of the proteins were performed by the methods described previously (*20*, *21*). The fractions with the A_{Soret} to A_{280} ratio greater than 1.5 were used for further experiments. We used an extinction coefficient of 102 $mM^{-1}cm^{-1}$ at 391 nm to estimate the concentration of the ferric camphor-bound $P450_{cam}$ (*22*). Pdx and PdR were expressed in *E. coli* and were purified by the method of Gunsalus and Wagner (*22*) with some minor modifications (*23*). The purified Pdx and PdR employed in this study had ratios of A_{325}/A_{280} and A_{455}/A_{280} greater than 0.62 and 0.12, respectively. Concentrations of Pdx and PdR were calculated using extinction coefficients of 10.4 $mM^{-1}cm^{-1}$ at 455 nm and 10 $mM^{-1}cm^{-1}$ at 454 nm, respectively (*22*).

Spectroscopic Measurements. UV/vis absorption spectra of the proteins were recorded with a Perkin-Elmer UV/vis spectrometer (Lambda 18). The measurements of EPR spectra were performed by the method of Shimada et al. (*24*). The EPR spectra were measured on a Varian E-12 spectrometer equipped with an Oxford EPR-900 liquid helium cryostat. The microwave frequency was X-band (9.22 GHz), and the microwave power was 5 mW. We prepared solutions of 200 μM Pdx in the absence and presence of 200 μM $P450_{cam}$ in 50 mM potassium phosphate at pH 7.4 (KP_i buffer) containing 50 mM KCl and 1 mM camphor. The solutions (100 μL) were transferred into a screw-topped EPR tube, and the samples were degassed by evacuation and subsequent flushing with oxygen-free nitrogen gas. A small amount of sodium dithionite was added into the sample tube containing Pdx and $P450_{cam}$ to reduce the proteins, and then CO gas was introduced. The EPR measurements of the complex between the ferrous−CO form of $P450_{cam}$ and reduced Pdx were carried out at 35 K.

Resonance Raman spectra were obtained using a spectrometer (Ritsu, DG-1000) equipped with a liquid nitrogen cooled CCD detector (Astromed CCD3200) and a holographic notch filter. All spectra were taken at the ambient temperature using a quartz spinning cell. The frequencies of Raman lines were calibrated with indene and ferrocyanide as standards. The sample concentration was 30 μM for P450s in the KP_i buffer containing 1 mM camphor. The Fe−S stretching mode of ferric P450s was detected by 351 nm excitation from a Kr ion laser (Spectra Physics, Model 2016). The ferrous samples were generated by addition of 1 μL of ca. 100 mM dithionite solution to 50 μL of the ferric samples in the anaerobic condition. The ferrous−CO adducts were prepared by flushing CO gas to the ferrous samples. We used the 441.6 nm excitation from a He−Cd laser (Kinmon Electronics, CCDR80SG) to observe the Fe−CO and FeC−O stretching modes. The Fe−CO stretching modes of the P450s were also measured in the presence of 60 μM reduced Pdx.

Redox Potential Measurements. Measurements of the oxidation−reduction potential for $P450_{cam}$ and its mutants were performed by use of the platinum electrode calibrated with phenosafranine ($E_0 = -252$ mV) (*25*). About 3 mL of the KP_i buffer containing 100 mM KCl, 1 mM camphor, and 50 mM EDTA was injected into the special cell and allowed to sit under argon atmosphere at room temperature for about 20 min. Phenosafranine, safranine T, benzyl viologen, and α-hydroxyphenazine were added as mediators. An oxygen-scavenging system composed of 60 mM glucose, 0.1 mg/mL glucose oxidase, and 3000 units/mL catalase was added to the solution to ensure the anaerobiosis (*26*, *27*). $P450_{cam}$ was subsequently injected into the solution to the final concentration of ca. 10 μM ($A_{Soret} = 1.0$). The preparations of the above solutions were conducted in the dark to avoid photoreduction of $P450_{cam}$. Ferric $P450_{cam}$ was partially reduced by illuminating the sample with a white tungsten lump (150 W) at 25 °C. After the irradiation, the absorbance at 391 nm and the electrode potential were recorded. This process was repeated until the protein samples could not be reduced by the irradiation; that is, the absorbance at 391 nm was not further changed (*25*). The midpoint potential (E_0) was obtained by using the Nernst equation (*28*):

$$E_{obs} = E_0 + (RT/nF)\ln([\text{oxidized P450}_{cam}]/[\text{reduced P450}_{cam}]) \quad (1)$$

where n and F denote the number of electrons involved in the redox reaction and the Faraday constant, respectively.

The temperature dependence of the reduction potentials was examined by measuring the potentials at 10, 25, and 35 °C. All potentials were corrected by the temperature dependence of the Ag/AgCl reference electrode (*29*) and were recalculated with reference to NHE.

Camphor Hydroxylation Activity Measurements. Catalytic activities of camphor hydroxylation for wild-type $P450_{cam}$ and the Gln360 mutants were evaluated by the NADH consumption rates (*30*). The assay mixture (2 mL) contained 0.5 μM $P450_{cam}$, 5 μM Pdx, 0.5 μM PdR, and 200 μM NADH in the KP_i buffer containing 100 mM KCl and 1 mM camphor (*14*, *20*). The reaction was initiated by the addition of the P450 samples, and the NADH consumption rate was determined by monitoring the decrease in the absorbance at 340 nm at 25 °C. The camphor-dependent NADH consumption was linear against time, and the rate was calculated with an extinction coefficient of 6.22 mM^{-1} cm^{-1} for NADH. After no further change in the absorbance at 340 nm was confirmed, the hydroxylation product was quantitated by a gas chromatograph equipped with a flame ionization detector (Shimadzu, GC-18A) and a DB-1701 column (J & W Scientific).

The yield of the hydrogen peroxide production was determined by the method based on the Fenton reaction (*31*, *32*) as shown in Scheme 1. In this method, 1 mL of 3% trichloroacetic acid was added to the reaction mixture. After 15 min, the solution was centrifuged, and then 500 μL of 10 M ferrous ammonium sulfate and 100 μL of 0.5 M KSCN were added to 500 μL of the supernatant. After 2 min, the absorbance at 480 nm was measured with a spectrometer, and the formation of hydrogen peroxide was calculated by using a standard curve based on the stock solutions of hydrogen peroxide (10−200 μM).

Scheme 1

$$H_2O_2 + Fe^{2+} \rightarrow Fe^{3+} + HO^- + \cdot OH$$

Measurements of the First Electron Transfer Rate. The first ET rates, the reduction rates of the ferric P450 samples by reduced Pdx, were measured according to the reported method (*26*, *33*). The standard buffer (3 mL) containing 2 μM ferric P450 samples and 3−30 μM oxidized Pdx was allowed to sit under CO atmosphere for about 20 min. An oxygen scavenging system composed of glucose, glucose oxidase, and catalase (*26*, *27*) was added to the solutions to ensure anaerobiosis. NADH (360 μM) and a catalytic amount of PdR (about 0.1 μM) were added to the solution of oxidized Pdx under CO atmosphere to obtain the reduced form of Pdx. The reduction of oxidized Pdx was monitored by the absorbance changes at 455 and 540 nm with a UV/vis spectrometer. The P450 solution was transferred to one of the reservoirs of the stopped-flow apparatus (UNISOKU) with an OLIS data acquisition system (OLIS RMS 1000, OLIS Inc.), and the reduced Pdx solution was transferred into the other reservoir. The reaction was started by mixing the two solutions and followed by measuring the formation of the ferrous−CO form of the P450 sample at 446 nm. All measurements were carried out at 25 °C.

Scheme 2

$$A + B \underset{k_{-1}}{\overset{k_1}{\rightleftharpoons}} C \underset{k_{-2}}{\overset{k_2}{\rightleftharpoons}} D$$

The reduction of the ferric P450 sample by reduced Pdx can be represented by a two-step model as shown in Scheme 2 (*26*). In the present experiment, A and B correspond to the ferric P450 sample and reduced Pdx, respectively, and C is the complex of the ferric enzyme with reduced Pdx. D represents the ferrous enzyme−oxidized Pdx complex. The ferrous enzyme is immediately trapped as its CO adduct in this experimental condition (*26*). Since the conversion from D to C is completely inhibited due to the strong affinity of CO to the ferrous form, we can assume $k_{-2} = 0$ for Scheme 2. In this case, the ET reaction follows the Michaelis−Menten-type mechanism, and the dissociation constant can be estimated by eq 2 and k_2 can be calculated from the

$$K_m = (k_{-1} + k_2)/k_1 \quad (2)$$

dependence of the formation rate of the CO adduct on the concentration of Pdx.

Measurements of the Second Electron Transfer Rate. The second ET rates, the reduction rates of the oxy adducts by reduced Pdx, were assessed by the previously reported procedure (*27*, *34*). Two milliliters of 10 μM ferric enzyme was allowed to sit under an argon atmosphere for about 20 min. The ferrous enzyme was prepared by careful addition of a minimal volume of ca. 20 mM sodium dithionite solution. Formation of the ferrous enzyme was confirmed by a UV/vis spectrometer. The oxy adduct was prepared by manually mixing the ferrous solution with an equal amount of air-saturated buffer at 4 °C and was immediately transferred to the reservoir of the stopped-flow apparatus. The reduced Pdx was prepared as described above. The reduction of the oxy adduct by reduced Pdx was started by mixing the two solutions at 4 °C and followed by measuring the formation of the ferric enzyme at 391 nm. The rapid-scan spectra were measured by the same apparatus used for the first ET measurements.

In the second ET reaction, A and B in Scheme 2 represent the oxy adduct and reduced Pdx, respectively. Since the hydroxylation reaction immediately proceeds after the ET from reduced Pdx, we can also assume that component D, the reduced oxy-$P450_{cam}$−oxidized Pdx complex, does not convert to component C, the oxy-$P450_{cam}$−reduced Pdx complex (*13*). Therefore, the second ET reaction can also be analyzed by the Michaelis−Menten-type mechanism.

RESULTS

Mutational Effects on the Structures of P450s. To assess the structural perturbation on the heme environment by the mutations, we utilized UV/vis and resonance Raman spectroscopies. The UV/visible absorption spectra of the mutants in the ferric, ferrous, and CO-bound states were almost indistinguishable from those of wild type (data not shown). Resonance Raman lines of the heme skeletal modes of the mutants were also the same as those of the wild-type enzyme (data not shown). However, the Fe−S, Fe−CO, and FeC−O stretching frequencies were shifted by the mutations (Table 1). The Fe−S stretching frequency was upshifted by ∼1 cm^{-1}, while the 1−3 and 2−5 cm^{-1} downshifts were found for the Fe−CO and FeC−O stretching frequencies, respectively. The low-frequency shifts in both the Fe−CO and FeC−O stretching modes indicate the increased CO−π^* back-donation by the enhanced electron donation of the Fe−S

Table 1: Fe−S, Fe−CO, and FeC−O Stretching Frequencies (cm^{-1}) of P450s

protein	ν_{Fe-S}	ν_{Fe-CO}	ν_{FeC-O}
wild type	351	484	1940
Q360E	352	481	1935
Q360K	351	483	1938
Q360L	352	483 (*18*)	1936 (*18*)

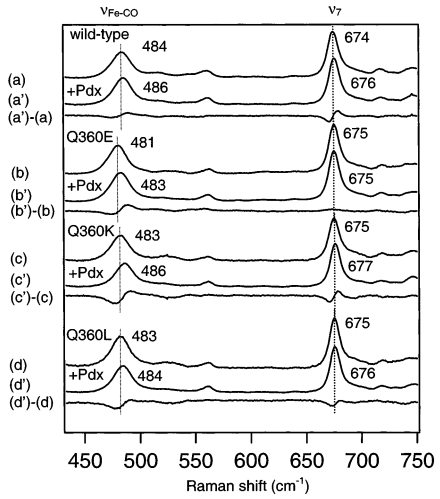

FIGURE 3: Resonance Raman spectra of the ferrous−CO forms of $P450_{cam}$ in the absence and presence of reduced Pdx by 441.6 nm excitation at room temperature. Traces a, b, c, and d represent resonance Raman spectra of wild-type $P450_{cam}$, Q360E, Q360K, and Q360L, respectively, in the absence of reduced Pdx. Traces a′, b′, c′, and d′ show resonance Raman spectra of the respective enzymes in the presence of reduced Pdx. Traces a′ − a, b′ − b, c′ − c, and d′ − d show the difference spectra of the respective enzymes. The samples were dissolved in 50 mM potassium phosphate buffer at pH 7.4 containing 1 mM camphor.

bond (*35*). However, the alterations of these stretching modes are slight and demonstrate the small structural perturbations in the heme coordination and environmental structures of the mutants.

Mutational Effects on the Structures of the $P450_{cam}$−Pdx Complex. Upon the complex formation of $P450_{cam}$ with Pdx, some structural rearrangements in both of the proteins have been reported (*24*, *36*−*42*), which have been thought to reflect the formation of the specific complex between $P450_{cam}$ and Pdx. The structural changes on the $P450_{cam}$ side by the binding of Pdx are evident in the Fe−CO stretching and the porphyrin in-plane ν_7 modes of the resonance Raman spectra (*37*, *42*). The Fe−CO stretching and ν_7 modes in the ferrous−CO form of $P450_{cam}$ are upshifted by 2 and 1 cm^{-1}, respectively, upon the binding of reduced Pdx (*37*, *42*). As clearly shown in Figure 3, the difference between the spectra taken in the presence and absence of Pdx demonstrated upshifts in both the Fe−CO stretching and ν_7 modes for all three mutants upon the Pdx binding. The spectral changes for the Gln360 mutants by binding Pdx were similar to those of wild-type $P450_{cam}$, which indicate that the mutations at Gln360 do not inhibit the conformational changes of $P450_{cam}$ by the complexation with Pdx.

The effects of the Gln360 mutations on the structural rearrangements of Pdx upon the binding of $P450_{cam}$ were also examined by EPR spectra. The EPR spectrum of reduced Pdx (Figure 4a) exhibits $g_{||}$ and $g_{\perp}$ signals at 2.02 and 1.94, respectively (*43*) (Figure 4a). The $g_{\perp}$ region was reported to

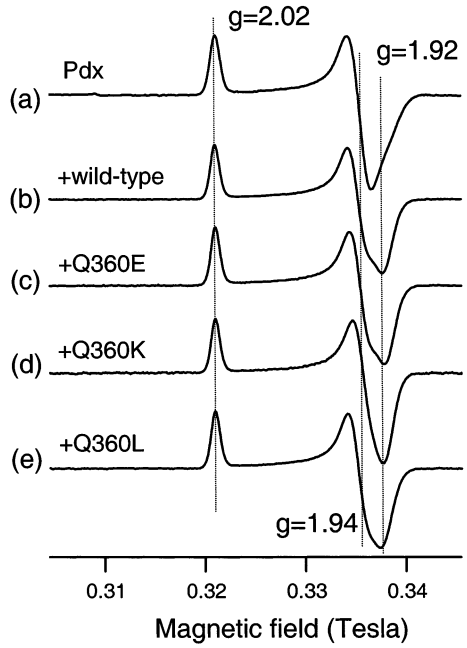

FIGURE 4: EPR spectra of reduced Pdx in the absence of $P450_{cam}$ (a) and in the presence of the ferrous−CO forms of wild-type $P450_{cam}$ (b), Q360E (c), Q360K (d), and Q360L (e) at 35 K. The samples were dissolved in 50 mM potassium phosphate buffer at pH 7.4 containing 50 mM KCl and 1 mM camphor.

Table 2: NADH Consumption Rates and Product Formations of P450s

protein	NADH consumption rate (μM/min)	product/NADH consumed (%)	
		ROH[a]	H_2O_2
wild type	319	100	1.8
Q360E	39	82	5.7
Q360K	379	93	2.4
Q360L	244	94	3.7

[a] ROH represents a hydroxylation substrate, 5-*exo*-camphor.

be modulated by the addition of ferrous−CO $P450_{cam}$ (Figure 4b) (*24*). The Gln360 mutants (Figure 4c−e) also showed similar spectral changes in the $g_{\perp}$ region. In sharp contrast to the Gln360 mutants, the EPR spectral changes for the Arg112 mutants, of which the mutation site is located at the putative Pdx binding site, were quite different from those for the wild-type enzyme (*24*, *44*), and the conformational changes by the Pdx binding in the Arg112 mutants are highly perturbed. We conclude that the mutational effects of Gln360 on the structure of the specific complex between the ferrous−CO adducts of $P450_{cam}$ and reduced Pdx are rather small compared with those of the Arg112 mutants.

Camphor Hydroxylation Activity. To examine the mutational effects on the activity of $P450_{cam}$, the consumption rates of NADH were measured in the reconstituted system containing $P450_{cam}$, Pdx, and PdR (*30*). The NADH consumption rates for the wild-type and mutant enzymes are summarized in Table 2. As listed in Table 2, the drastic reduction in the rate was only found for the Q360E mutant. The moderate decrease in the consumption rate was observed in the Leu mutant, while the Lys mutant exhibited a slightly enhanced rate. The drastic decrease in the rate for the Q360E mutant is rather surprising, because both the EPR and resonance Raman spectroscopies indicated that the structure of the mutant−Pdx complex was similar to that of the wild-

type enzyme−Pdx complex. Since the rate-limiting process for the NADH consumption is the first ET reaction, the ET process from reduced Pdx to the ferric state of $P450_{cam}$, these results indicate that Gln360 plays functional roles in the first ET reaction.

To confirm that the effect of the mutations at Gln360 on the NADH consumption is due to the perturbations in the first ET process, we measured the yields of the hydroxylation product of *d*-camphor, 5-*exo*-hydroxycamphor, and hydrogen peroxide. These yields sensitively reflect the efficiency of the substrate hydroxylation step. For example, the product analysis for the hydroxylation reaction of the Thr252 mutants, which have mutations near the dioxygen binding site, has revealed the increased formation of hydrogen peroxide to 45−88% of NADH consumed (*45*). The mutations at Thr252 perturb the distribution of water molecules in the heme pocket of $P450_{cam}$, resulting in the slow oxygen transfer rates to the substrate and the enhanced release of hydrogen peroxide (*45*−*47*). We listed the yields of hydroxycamphor and hydrogen peroxide relative to the consumed amount of NADH of the Gln360 mutants in Table 2. The yields of hydrogen peroxide for the mutant enzymes were less than 6%. Furthermore, 5-*exo*-hydroxycamphor was detected as the unique hydroxylated product of *d*-camphor in the reconstituted systems of the mutants. These results indicate that the mutations of Gln360 did not seriously affect the hydroxylation of the substrate. Thus, the modulations in the first ET rate are responsible for the effect of the NADH consumption rate by the mutations at Gln360.

The First Electron Transfer. To quantitatively investigate the mutational effects on the ET reaction, we measured the first ET rate in the single turnover reaction. The first ET rate can be monitored as the formation rate of the ferrous CO derivative of $P450_{cam}$ after the rapid mixing of ferric $P450_{cam}$ and reduced Pdx in the presence of CO (*26*, *33*). Figure 5A shows the typical time course of the reaction observed at the Soret maximum of the ferrous−CO form (446 nm) for the Q360E mutant. The circles and curve represent experimental data points and their single exponential fitting, respectively. The residuals from the single exponential fitting shown above were random, implying that the reaction followed first-order kinetics. The kinetic traces for the other mutants also showed first-order kinetics (data not shown).

The apparent rate constants (k_{obs1}) at the various concentrations of Pdx were estimated from the fitting curves and plotted as a function of the Pdx concentration (Figure 5B). The Q360E exhibited smaller k_{obs1} values than those of other mutants and wild-type $P450_{cam}$. The k_{obs1} values for the Q360L mutant were also smaller than those of the wild-type enzyme but much larger than those of the Q360E mutant. A slight but significant enhancement in k_{obs1} was observed for the Q360K mutant. The order of the k_{obs1} values corresponds to that of the NADH consumption rates, confirming that the observed turnover rates correlate to the first ET rates.

The values of the Michaelis constant (K_{m1}) and the ET rate (k_{ET1}) for the first ET process were estimated by fitting the k_{obs1} values using eq 3 (*27*). The estimated parameters

$$k_{obs1} = \frac{k_{ET1}[Pdx]}{[Pdx] + K_{m1}} \qquad (3)$$

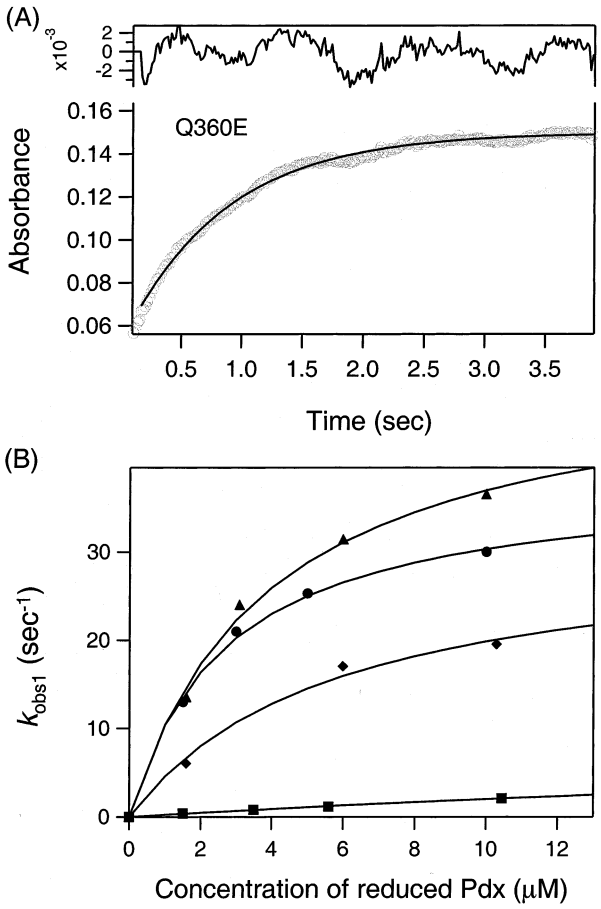

FIGURE 5: (A) Time course for the first electron transfer reaction in Q360E. The measurement was carried out at 446 nm by mixing ferric $P450_{cam}$ (2 μM) and reduced Pdx (10 μM) at 25 °C in 50 mM potassium phosphate buffer at pH 7.4 containing 100 mM KCl and 1 mM camphor. The circles and curve represent the experimental data points and the single exponential fitting, respectively. The residuals of the fitting are shown in the top of the time course. (B) k_{obs1} for the first ET reaction of wild-type $P450_{cam}$ (●), Q360E (■), Q360K (▲), and Q360L (◆) as a function of the concentration of Pdx. The solid curves represent the least-squares fits by eq 3.

Table 3: Kinetic and Equilibrium Parameters of the First and Second Electron Transfer Reactions

protein	K_{m1} (μM)	k_{ET1} (s^{-1})	K_{m2} (μM)	k_{ET2} (s^{-1})	redox potential (mV)[c]
wild type	2.6 ± 0.28	35 ± 1.5	4.4 ± 1.2	139 ± 11	−134
Q360E	52 ± 18.1	5.4 ± 3.7	14 ± 6.5	42 ± 8.1	−203
Q360K	3.9 ± 0.61	53 ± 3.3	9.2 ± 2.8	130 ± 16	−151
Q360L	5.8 ± 2.0	23 ± 4.9	2.9 ± 3.0	83 ± 13	−180[e]
wild type[d]	0.19[a]	42	—[b]	—	−138
R112K[d]	4.4[a]	18	—	—	−162
R112C[d]	480[a]	4.0	—	—	−182
R112M[d]	470[a]	1.3	—	—	−200
R112Y[d]	110[a]	0.16	—	—	−195

[a] Dissociation constant, $K_d = k_{-1}/k_1$ (μM). [b] A dash indicates that kinetic parameters of the second ET reaction were not measured for the Arg112 mutants. [c] The redox potentials vs NHE for the Fe^{3+}/Fe^{2+} couple. [d] From ref *13*. [e] From ref *18*.

are summarized in Table 3. K_{m1} for the wild-type enzyme was 2.6 μM, which is virtually the same as that reported previously (*13*). All of the mutants had larger K_{m1} values than the wild-type enzyme, showing that the mutations at position 360 decrease the affinity to Pdx. As expected, the most prominent increase in K_{m1} was found for the Q360E

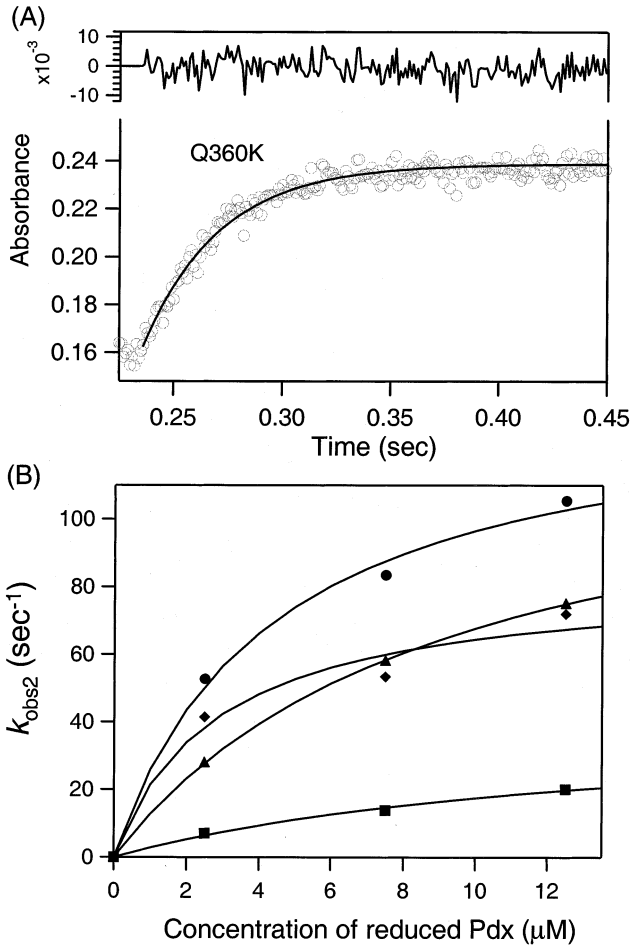

FIGURE 6: (A) Time course observed for the second electron transfer reaction in Q360K. The measurement was carried out at 392 nm by mixing oxy-P450$_{cam}$ (2.5 μM) and reduced Pdx (5 μM) at 4 °C in 50 mM potassium phosphate buffer at pH 7.4 containing 100 mM KCl and 1 mM camphor. The circles and curve represent the experimental data points and the single exponential fitting, respectively. The residuals of the fitting are shown in the top of the time course. (B) k_{obs2} for the second ET reaction of wild-type P450$_{cam}$ (●), Q360E (■), Q360K (▲), and Q360L (◆) as a function of the concentration of Pdx. The solid curves represent the least-squares fits by eq 3.

mutant, and the K_{m1} values for other two mutants were not so drastically increased. The intracomplex ET rates (k_{ET1}) were also perturbed by the mutations. The k_{ET1} value for the Q360E mutant was highly retarded; however, the k_{ET1} value for the Q360K mutant was accelerated as found for the NADH consumption rate. The significant alterations in the kinetic parameters by the mutations of Gln360 indicate that Gln360 modulates the first ET process in the catalytic cycle of P450$_{cam}$ (*13*).

The Second Electron Transfer. We also examined the mutational effects on the second ET reaction, the reduction rate of oxy-P450$_{cam}$ by reduced Pdx. The second ET rate was assessed by monitoring the formation of the ferric enzyme after mixing oxy-P450$_{cam}$ and reduced Pdx (*13*, *27*). Figure 6A shows the absorbance change at 391 nm, the Soret peak of the ferric form of Q360K, after mixing. The circles and curve represent the experimental data points and their single exponential fitting, respectively. All mutant enzymes followed first-order kinetics as observed for the first ET reaction. The apparent rate constants (k_{obs2}) are plotted against the concentrations of Pdx in Figure 6B.

The k_{obs2} values were also fitted by eq 3 to estimate the kinetic parameters, Michaelis constant (K_{m2}), and intracomplex ET rate (k_{ET2}) for the second ET reaction (*27*, *45*). Table 3 lists K_{m2} and k_{ET2} for the mutants and the wild-type enzyme. The kinetic parameters for the wild-type enzyme were similar to those obtained previously (*13*, *34*). Although the Q360E mutant gave the smallest k_{ET2} among the mutants, the deviation from k_{ET2} of the wild-type enzyme (3.2-fold) was much smaller than the deviations observed in k_{ET1} (6.5-fold). The Q360L mutant, whose affinity to Pdx in the first ET process was decreased, showed slightly increased affinity to Pdx in the second ET process. The reduced mutational effects on the second ET process were also evident in K_{m2}. We conclude that the mutation of Glu360 perturbs the second ET reaction from reduced Pdx to oxygenated P450$_{cam}$, but the mutational effects were smaller than those on the first ET process.

Redox Potential of the Gln360 Mutants. As shown in the previous section, the mutations of Gln360 affected both the first and second ET reactions. To gain further insight into the mutational effects on the ET processes, the redox potentials of the heme iron, one of the factors that regulate the ET reactions, were measured for the mutant enzymes. The monitored electrode potentials against the percentage of reduced P450s were fitted by the Nernst equation, and the redox potentials of the Fe^{2+}/Fe^{3+} couple were estimated (*25*). The redox potential of wild-type P450$_{cam}$ at 25 °C (−134 mV) was in good agreement with the value reported by Unno et al. (*13*). The redox potentials of the mutant enzymes were −203, −151, and −180 mV for Q360E, Q360K, and Q360L (*18*), respectively, at 25 °C (Table 3). In contrast to the small structural perturbation in the heme environments, the shifts of the redox potentials in the mutants were distinct. The redox potential for the Q360E mutant (−203 mV) was very low and close to the midpoint potential of Pdx (−215 mV) (*25*). On the other hand, the mutation of Gln360 to Leu or Lys resulted in less negatively shifted redox potentials. The introduction of the negative charge into position 360 drastically shifted the redox potential to the negative side, which would be the major factor for the reduced ET rate in the Q360E mutant.

To analyze the mutational effects on the redox potential, we estimated the standard entropy and enthalpy for the redox reaction of P450$_{cam}$ with Pdx. Figure 7 shows the temperature dependence of the redox potentials of wild-type and mutant P450$_{cam}$s. It should be noted that the plots of the redox potential versus temperature are linear for all samples in the range between 10 and 35 °C. The slope of the reduction potential versus temperature is related to the standard entropy ($\Delta S°'$) as shown in eq 4 (*48*). The free energy change ($\Delta G°'$)

$$\Delta S°' = nF(\delta E_0/\delta T)_P \quad (4)$$

and the standard enthalpy ($\Delta H°'$) can be determined by eqs 5 and 6, where E_{25} is the redox potential vs NHE at 25 °C.

$$\Delta G°' = -nFE_{25} \quad (5)$$

$$\Delta H°' = \Delta G°' + T\Delta S°' \quad (6)$$

The thermodynamic parameters obtained for the wild-type and mutant enzymes are compiled in Table 4. The $\Delta S°'$ value

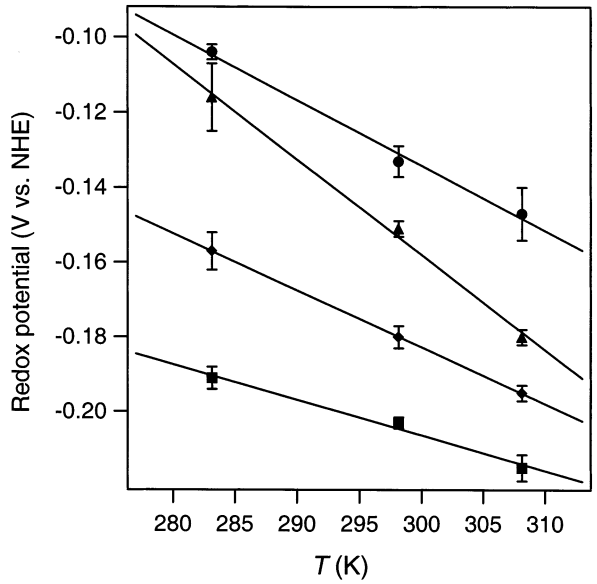

FIGURE 7: Temperature dependence of the reduction potentials of wild-type $P450_{cam}$ (●), Q360E (■), Q360K (▲), and Q360L (◆). The values were obtained in 50 mM potassium phosphate buffer at pH 7.4 containing 100 mM KCl, 1 mM camphor, and 50 mM EDTA. Error bars were calculated from the standard deviations. The lines represent the least-squares linear fits of the experimental data.

Table 4: Thermodynamic Parameters of the Redox Reaction for Wild-Type $P450_{cam}$ and $P450_{cam}$ Mutants at 25 °C

protein	$\Delta S^{\circ\prime}$ (J mol^{-1} K^{-1})	$T\Delta S^{\circ\prime}$ (kJ mol^{-1})	$\Delta H^{\circ\prime}$ (kJ mol^{-1})	$\Delta G^{\circ\prime}$ (kJ mol^{-1})
wild type	-168 ± 14	-50.1 ± 4.2	-37.3 ± 4.6	12.8 ± 0.4
Q360E	-91 ± 11	-27.1 ± 3.3	-8.1 ± 3.4	19.0 ± 0.1
Q360K	-245 ± 15	-73.0 ± 4.5	-58.4 ± 4.7	14.6 ± 0.2
Q360L	-147 ± 11	-43.8 ± 3.3	-26.4 ± 3.6	17.4 ± 0.3

for the wild-type enzyme was negative, -168 ± 14 J mol^{-1} K^{-1}, which reflects unfavorable changes upon reduction. In contrast to $\Delta S^{\circ\prime}$, the $\Delta H^{\circ\prime}$ value for the wild-type enzyme (37.3 ± 4.6 kJ mol^{-1}) is favorable for the reduction. The reduction reaction of the heme iron in $P450_{cam}$ is, therefore, an enthalpy-driven reaction. Although $\Delta S^{\circ\prime}$ and $\Delta H^{\circ\prime}$ for the Gln360 mutants were also negative as observed for the wild-type enzyme, small but significant deviations from those of the wild-type enzyme were detected. The $\Delta S^{\circ\prime}$ and $\Delta H^{\circ\prime}$ values of the Q360K mutant were shifted to the negative side, while the positive shifts of $\Delta S^{\circ\prime}$ and $\Delta H^{\circ\prime}$ were observed for the Q360E and Q360L mutants. The positively shifted $\Delta G^{\circ\prime}$ for the mutants, corresponding to the lowered redox potential, is due to large negative $\Delta S^{\circ\prime}$ for the Q360K mutant and small negative $\Delta H^{\circ\prime}$ for the Q360E and Q360L mutants. The mutation at Gln360 affects both of the enthalpic and entropic components for the redox reaction between $P450_{cam}$ and Pdx.

DISCUSSION

Our current results show that the effects of the mutations at Gln360 on the structures of $P450_{cam}$ and the complex with Pdx were relatively small compared with the reported effects of the mutations of Arg109 and Arg112 (*24*, *44*); however, the mutational effects at Gln360 on the kinetic parameters of the ET reactions between $P450_{cam}$ and Pdx were significant. Particularly, the mutational effects of Gln360 on the redox potential of the heme iron in $P450_{cam}$ were comparable to those of the Arg112 mutants. For example, the Gln360 → Glu mutation lowered its redox potential by 70 mV, which is larger than the largest changes of the redox potential observed for the Arg112 mutants (−62 mV for Arg112 → Met). In the following sections, we will discuss the mutational effects on (i) the formation of the ET complex and the intracomplex ET rate and (ii) the redox potential. Finally, we will propose the functional roles of Gln360 in the ET reactions between $P450_{cam}$ and Pdx.

Mutational Effects on the ET Complex and the Intracomplex Electron Transfer Rates (k_{ET}). According to the model structure for the complex between $P450_{cam}$ and Pdx hypothesized by Pochapsky et al., the side chain of Gln360 is hydrogen bonded to Cys39 of Pdx (*16*), and the disruption of the hydrogen bond by the mutations of Gln360 should result in a decrease of the affinity to Pdx. However, the mutational effects on the affinity to Pdx ($\sim 1/20$ of wild type), the K_m value, were not so drastic. In contrast, the mutations of Arg112 inhibit the formation of the specific complex and drastically decrease the affinity with Pdx to $1/2500-1/25$ of that of wild-type $P450_{cam}$ (*13*). Thus, Gln360 is one of the amino acid residues in the Pdx binding site to form interactions with Pdx, but its contribution to the specific recognition and formation of the $P450_{cam}$−Pdx complex is not as essential as that of Arg112. We, therefore, suggest that the putative hydrogen bond between Gln360 and Cys39 of Pdx is weak and the disruption of the hydrogen bond might be compensated by the other interactions, or Gln360 interacts with Pdx not by the formation of the hydrogen bond with Cys39.

The mutational effects on the affinity to Pdx are reasonable in comparison with the mutational studies about other protein−protein complexes. Mei et al. performed the disruption of the hydrogen bonds in the cytochrome *c* peroxidase (C*c*P)−cytochrome *c* complex by single mutations of C*c*P and investigated the mutational effects on the dissociation constant of the C*c*P−cytochrome *c* complex (*49*). Although these mutations also reduce the electrostatic interaction between C*c*P and cytochrome *c*, the disruption of a single hydrogen bond increases the dissociation constant to 1.5−22-fold of that of wild-type C*c*P. Hiraga and Yutani reported that the disruption of a single hydrogen bond between the α and β subunits of tryptophan synthase increases the dissociation constant of their complex to 1.2−33-fold of that of wild-type tryptophan synthase (*50*). In contrast, the increase of the dissociation constants for the first and second ET reactions in the Pdx−Q360L complex were only 2.2- and 0.66-fold of those of the wild-type enzyme, respectively. This observation supports the minor contribution of the hydrogen bond between Gln360 and Cys39 to the complex formation of $P450_{cam}$ with Pdx.

The current experimental results of the ET rates from reduced Pdx to ferric $P450_{cam}$, however, clearly indicate that Gln360 is contained in the amino acid residues essential for the ET processes. Although the mutational effects on the structures of $P450_{cam}$ and the $P450_{cam}$−Pdx complex were small, the most prominent effect of the mutations of Gln360 was the negatively shifted redox potentials. To confirm that the alteration of the ET rate can be explained from the redox potentials, we will quantitatively analyze the ET reactions

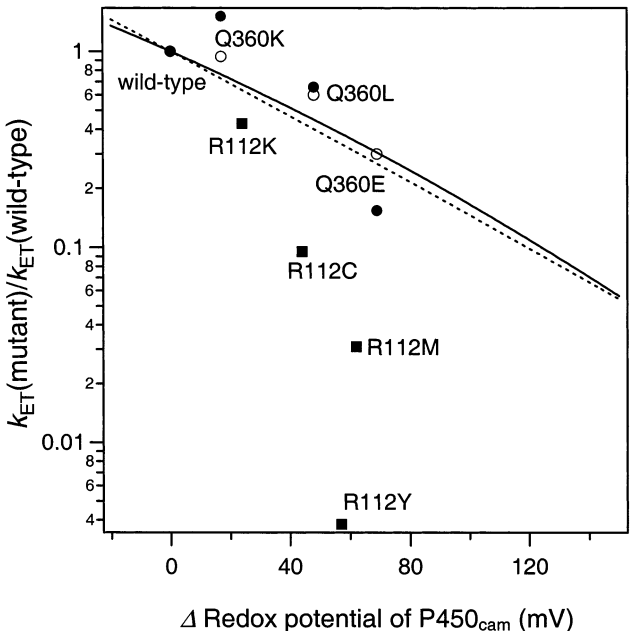

FIGURE 8: Correlation between the redox potentials of the Gln360 mutants and the intracomplex ET rates for the first and second ET reactions. Δ redox potential represents the difference in the redox potentials between the mutants and the wild-type enzyme. Closed circles represent the first ET rates, and open circles represent the second ET rates obtained in this study. Closed squares represent the first ET rates of the Arg112 mutants (*13*). Curves represent the calculated dependency of the ET rate on the redox potential based on the Marcus equation by use of 0.4 (solid curve) and 2.5 eV (dashed curve) as the values of λ.

using the Marcus equation (*51*). The Marcus equation (*51*) is given as

$$k_{ET} = \frac{4\pi^2 {H_{AB}}^2}{h(4\pi\lambda RT)^{1/2}} \exp\left[-\frac{(\Delta G^\circ + \lambda)^2}{4\lambda RT}\right] \qquad (7)$$

where k_{ET} is the intracomplex ET rate, h is Planck's constant, R is the gas constant, T is temperature, λ is the reorganization energy, ΔG° is the redox potential difference between donor and acceptor, and H_{AB} describes the degree of wave function overlap between the donor and the acceptor sites. Since H_{AB} is related to the distance between redox centers, d, k_{ET} is also expressed as (*52*)

$$k_{ET} = k_0 \exp[-\beta(d - d_0)] \exp\left[-\frac{(\Delta G^\circ + \lambda)^2}{4\lambda RT}\right] \qquad (8)$$

In eq 8, k_0 is the characteristic frequency of the nuclei and is assigned to a value of 10^{13} s^{-1} (*52*). β is the electronic decay factor and is often approximated as 1.4 $Å^{-1}$ (*53*). To correlate the changes in the ET rates with those of the redox potentials, k_{ET1} was plotted against the redox potential of the mutants and wild-type enzyme, as displayed in Figure 8. The experimental data (closed and open circles in Figure 8) are compared with the simulation curves calculated from the Marcus equation (eq 8). The simulated curves were calculated by assuming that all parameters except for ΔG° are not perturbed by the mutations and that the redox potential of Pdx is −215 mV (*25*). Since λ for most of the physiological ET reactions falls within the range from 0.4 to 2.5 eV (*54*−*56*), we use 0.4 (solid line) and 2.5 eV (dashed line) as the values of λ for the simulation. As seen in Figure 8, the calculated k_{ET} monotonically decreases as the redox potential is negatively shifted. The Q360E and Q360L mutants exhibited small k_{ET1} with the negatively shifted redox potentials, which are qualitatively consistent with the calculated k_{ET1}. The largest deviation was observed for the Q360K mutant, but the deviation is within the factor of 2. Although the deviations of the observed k_{ET1} from the simulated curves imply that the mutations at Gln360 also affect other parameters except for the redox potential, the alterations of k_{ET1} by the mutations of Gln360 can almost be explained from the negative shifts of their redox potentials and suggest that Gln360 is not involved in the major ET pathway between $P450_{cam}$ and Pdx.

Contrary to the Q360E and Q360L mutants, accelerated k_{ET1} was observed for the Q360K mutant despite the negatively shifted redox potential, suggesting that the contributions of the alterations in other factors, except for the redox potentials, to k_{ET1} are enhanced by the introduction of Lys into position 360. For example, a deviation of 0.1 eV in the reorganization energy, λ, leads to 50% increases of k_{ET1}. Assuming that the distance between redox centers, d, is decreased by 0.5 Å, k_{ET1} would be accelerated to 1.5-fold of that of the original state. Although these perturbations on λ and/or d would be rather small, it is interesting that the perturbations are prominent only in the Lys-substituted mutant. One of the reasons for the perturbations on λ and/or d in the Q360K mutant would be the long and positively charged side chain of Lys. The side chain of the lysine residue at position 360 is located in the interface between $P450_{cam}$ and Pdx, whose steric hindrance and/or positive charge might induce positional rearrangements of the surrounding of the amino acid residues involved in the interactions between $P450_{cam}$ and Pdx.

In contrast to the rather small deviations of the first ET rate for the Gln360 mutants from the theoretical curves, a series of the Arg112 mutants (closed square in Figure 8) exhibit the large deviations of the first ET rate (*13*). While the redox potential of the R112M mutant (−200 mV) is comparable to that of the Q360E mutants (−203 mV), the ET rate of the R112M mutant is less than 5% of that of the wild-type enzyme, which is much slower than those expected from the Marcus equation (30%) and observed for the Q360E mutant (15%). Such large deviations of the ET rates from the Marcus equation imply that the mutations at Arg112 affect not only the redox potentials but also other factors such as λ and d for the ET complex between $P450_{cam}$ and Pdx. The changes of λ and/or d by the mutations of Arg112 are the likely explanations, since the EPR-detectable conformational change in the $P450_{cam}$−Pdx complex for the Arg112 → Lys mutant was significantly different from that observed in the wild-type enzyme (*24*, *44*). We therefore conclude that the functional significance of Gln360 on the first ET process is different from that of Arg112. Arg112 is crucial for the formation of the specific ET complex between $P450_{cam}$ and Pdx. On the other hand, the primary role of Gln360 in the ET reaction with Pdx is not the complex formation but the regulation of the redox potentials of the heme iron.

The dependence of k_{ET2} on the redox potentials is almost in line with the theoretical curve calculated for the first ET process by the Marcus equation (Figure 8). Although the

redox potential of oxy-$P450_{cam}$ cannot be determined due to the instability of the oxygen adduct, the systematic studies on the redox potentials of mutant horseradish peroxidases have revealed the significant correlation among the redox potentials for the Fe^{3+}/Fe^{2+}, Fe^{4+}(compound II)/Fe^{3+}, and Fe^{5+}(compound I)/Fe^{4+}(compound II) couples (*57*). It is, therefore, likely that the redox potentials for the dioxygen adducts of the $P450_{cam}$ mutants are parallel to those for the ferric state. In the second ET rate, the mutations of Gln360 also primarily affect the redox potentials, and other factors, such as λ and d, are less significantly affected.

It should be noted here that larger deviations of k_{ET} from the simulated curve are observed for the first ET process rather than the second ET process. The different redox potential dependence of k_{ET2} from that of k_{ET1} might reflect the difference in the interactions for the complex formation between the first and second ET processes. This suggestion is also supported by the difference of the mutational effects on the K_m value listed in Table 3. For example, the mutation of Gln360 to Glu increased the K_m value to 20-fold of that of wild type in the first ET reaction, although the K_m value in the second ET reaction was increased to 3-fold by the same mutation. As previously reported, the EPR spectrum of reduced Pdx in the $P450_{cam}$−Pdx complex is modulated by the binding of ligands such as CO, NO, and O_2 (*24*). Shimada et al. suggested that this spectral change is caused by the movement of the heme iron in $P450_{cam}$ from the out of plane position to the in plane position. The movement of the heme iron in $P450_{cam}$ could induce the structural rearrangement in the proximal side of $P450_{cam}$ through the axial Cys. Since the axial Cys interacts with Gln360 by the hydrogen-bonding network, the movement of the heme iron might evoke the positional change of Gln360. We propose that these structural changes accompanied by the movement of the heme iron would cause the dependence of the interactions between $P450_{cam}$ and Pdx on the redox state of $P450_{cam}$.

Roles of Gln360 in the ET Reactions between $P450_{cam}$ and Pdx. As discussed in the previous section, the primary effect of the mutations at Glu360 on the ET processes is on the redox potential of the heme iron. The temperature dependence of the redox potential for the Gln360 mutants delineates the functional role of Gln360. The variations of $\Delta H^{\circ\prime}$ by the mutations (−21.1 to +29.2 kJ mol^{-1}) were comparable to those of $T\Delta S^{\circ\prime}$ (−22.9 to +23.0 kJ mol^{-1}) as summarized in Table 4 and are derived from the structural changes by the mutations. From the crystal structure of ferric $P450_{cam}$, two hydrogen bonds are suggested to be formed between the axial ligand, Cys357, and Gln360 (*5*, *58*). One of the hydrogen bonds is a NH−S hydrogen bond between the main chain amide proton of Gln360 and the sulfhydryl group of Cys357. The side chain amide proton of Gln360 can also interact with the main chain carbonyl group of Cys357 (Figure 2). Since we have previously shown that the mutation of Gln360 to Leu did not seriously affect the NH−S bond between Gln360 and Cys357 (*18*), the positive shift of $\Delta H^{\circ\prime}$ observed for the Q360L mutant (about 11 kJ mol^{-1}) would be attributable to the loss of the hydrogen bond between the carbonyl group of cysteine and the amide group of Gln360. The variation in $\Delta H^{\circ\prime}$ for the Q360L mutant corresponds to the energy of a single hydrogen bond in proteins (12 kJ mol^{-1}) (*59*), which suggests that the hydrogen bond between Gln360 and Cys357 might be affected upon reduction. The $\Delta H^{\circ\prime}$ values for the other Gln360 mutants, Q360E and Q360K, are different from that for the Q360L mutant. In the Q360E mutant having a negative charge at position 360, $\Delta H^{\circ\prime}$ was further shifted to the positive side by 18 kJ mol^{-1}, compared with that of the Q360L mutant. In contrast, the introduction of a positive charge in the Q360K mutant shifted $\Delta H^{\circ\prime}$ to the negative side (21 kJ mol^{-1}). Thus, the alterations of the $\Delta H^{\circ\prime}$ values for the Gln360 mutants can be explained by the combination of the charge at the side chain of position 360 and the hydrogen-bonding interaction between the axial ligand and the side chain of position 360.

The mutational effects on the entropic component of the redox reaction are opposite to those on the enthalpic component. For instance, contrary to the positive contribution of $\Delta H^{\circ\prime}$ (21 kJ mol^{-1}) to the change of the redox potential for the Q360K mutant, $T\Delta S^{\circ\prime}$ was shifted to the negative side (23 kJ mol^{-1}). Such phenomenon was known as the enthalpy−entropy compensation and was similarly observed for the redox reactions of cytochromes (*60*) and blue copper proteins (*61*, *62*). These enthalpy−entropy compensation phenomena are likely the result of the mutational effects on the redox-dependent solvation properties of the protein (*60*). It should be noted here that the variations of $T\Delta S^{\circ\prime}$ by the mutations of Gln360 are larger than those obtained from the mutational studies in other proteins such as plastocyanin (*61*), azurin (*62*), ferredoxin (*63*), and high-potential iron protein (*64*). In the series of the mutational studies, only one of the mutants of azurin, His35 → Leu, exhibited the large variation of $T\Delta S^{\circ\prime}$(+19 kJ mol^{-1}), which is comparable to that of the Q360E mutant (+23 kJ mol^{-1}). It is known that the substitution of His35 of azurin induces the opening of the cavity near the metal site and enhances the accessibility of the redox center, copper, to the solvent (*65*). We, therefore, suggest that the mutations of Gln360 drastically alter the accessibility around position 360 to the solvent and vary the entropic component. Another possibility for the large variations of $T\Delta S^{\circ\prime}$ might be the mutational effect on the redox-dependent dynamics of Gln360 as observed for cytochrome b_5 (*66*). It is plausible that the mutation at 360 affects the positions of the charged residues on the protein surface, resulting in the alteration of the accessibility to the solvent around the residue at position 360 and the dynamics of the residue.

In summary, we observed significant effects of the mutation at Gln360 on both of the first and second ET reactions in the catalytic cycle of $P450_{cam}$. The mutations at Gln360 did not seriously affect the complex formation for the ET from Pdx, but the alterations of intracomplex ET rates by the mutations at Gln360 were significant, which can be primarily attributable to the shifts of the redox potentials. We can, therefore, conclude that Gln360 regulates the redox potential of the heme iron, thereby affecting the intracomplex ET rate in the $P450_{cam}$−Pdx complex.

ACKNOWLEDGMENT

We are indebted to Prof. Teizo Kitagawa (IMS, Okazaki) for kind permission to use the resonance Raman instrument. We are also grateful to Prof. Isao Taniguchi (Kumamoto University) for helpful advice on the measurement of the redox potential.

REFERENCES

1. Hollenberg, P. F. (1992) *FASEB J. 6*, 686−694.
2. Bernhardt, R., and Gunsalus, I. C. (1992) *Biochem. Biophys. Res. Commun. 187*, 310−317.
3. Lehnerer, M., Schulze, J., Bernhardt, R., and Hlavica, P. (1999) *Biochem. Biophys. Res. Commun. 254*, 83−87.
4. Jenkins, C. M., and Waterman, M. R. (1998) *Biochemistry 37*, 6106−6113.
5. Poulos, T. L., Finzel, B. C., and Howard, A. J. (1987) *J. Mol. Biol. 195*, 687−700.
6. Pochapsky, T. C., Jain, N. U., Kuti, M., Lyons, T. A., and Heymont, J. (1999) *Biochemistry 38*, 4681−4690.
7. Katagiri, M., Ganguli, B. N., and Gunsalus, I. C. (1968) *J. Biol. Chem. 243*, 3543−3546.
8. Lipscomb, J. D., Sligar, S. G., Namtvedt, M. J., and Gunsalus, I. C. (1976) *J. Biol. Chem. 251*, 1116−1124.
9. Stayton, P. S., and Sligar, S. G. (1990) *Biochemistry 29*, 7381−7386.
10. Koga, H., Sagara, Y., Yaoi, T., Tsujimura, M., Nakamura, K., Sekimizu, K., Makino, R., Shimada, H., Ishimura, Y., and Yura, K. (1993) *FEBS Lett. 331*, 109−113.
11. Nakamura, K., Horiuchi, T., Yasukochi, T., Sekimizu, K., Hara, T., and Sagara, Y. (1994) *Biochim. Biophys. Acta 1207*, 40−48.
12. Yasukochi, T., Okada, O., Hara, T., Sagara, Y., Sekimizu, K., and Horiuchi, T. (1994) *Biochim. Biophys. Acta 1204*, 84−90.
13. Unno, M., Shimada, H., Toba, Y., Makino, R., and Ishimura, Y. (1996) *J. Biol. Chem. 271*, 17869−17874.
14. Aoki, M., Ishimori, K., and Morishima, I. (1998) *Biochim. Biophys. Acta 1386*, 157−167.
15. Holden, M., Mayhew, M., Bunk, D., Roitberg, A., and Vilker, V. (1997) *J. Biol. Chem. 272*, 21720−21725.
16. Pochapsky, T. C., Lyons, T. A., Kazanis, S., Arakaki, T., and Ratnaswamy, G. (1996) *Biochimie 78*, 723−733.
17. Roitberg, A. E., Holden, M. J., Mayhew, M. P., Kurnikov, I. V., Beratan, D. N., and Vilker, V. L. (1998) *J. Am. Chem. Soc. 120*, 8927−8932.
18. Yoshioka, S., Tosha, T., Takahashi, S., Ishimori, K., Morishima, I., and Hori, H. (2002) *J. Am. Chem. Soc.* (in press).
19. Kunkel, T. A. (1985) *Proc. Natl. Acad. Sci. U.S.A. 82*, 488−492.
20. Yoshioka, S., Takahashi, S., Ishimori, K., and Morishima, I. (2000) *J. Inorg. Biochem. 81*, 141−151.
21. Yoshioka, S., Takahashi, S., Hori, H., Ishimori, K., and Morishima, I. (2001) *Eur. J. Biochem. 268*, 252−259.
22. Gunsalus, I. C., and Wagner, G. C. (1978) *Methods Enzymol. 52*, 166−188.
23. Aoki, M., Ishimori, K., Morishima, I., and Wada, Y. (1998) *Inorg. Chim. Acta 272*, 80−88.
24. Shimada, H., Nagano, S., Ariga, Y., Unno, M., Egawa, T., Hishiki, T., Ishimura, Y., Masuya, F., Obata, T., and Hori, H. (1999) *J. Biol. Chem. 274*, 9363−9369.
25. Makino, R., Iizuka, T., Sakaguchi, K., and Ishimura, Y. (1982) *Oxygenases and Oxygen Metabolism*, Academic Press, New York.
26. Hintz, M. J., and Peterson, J. A. (1981) *J. Biol. Chem. 256*, 6721−6728.
27. Brewer, C. B., and Peterson, J. A. (1988) *J. Biol. Chem. 263*, 791−798.
28. Yamada, H., Makino, R., and Yamazaki, I. (1975) *Arch. Biochem. Biophys. 169*, 344−353.
29. Janz, G. J. (1961) in *Reference Electrode. Theory and Practice*, Academic Press, New York.
30. Atkins, W. M., and Sligar, S. G. (1988) *J. Biol. Chem. 263*, 18842−18849.
31. Atkins, W. M., and Sligar, S. G. (1987) *J. Am. Chem. Soc. 109*, 3754−3760.
32. Loida, P. J., and Sligar, S. G. (1993) *Biochemistry 32*, 11530−11538.
33. Hintz, M. J., Mock, D. M., Peterson, L. L., Tuttle, K., and Peterson, J. A. (1982) *J. Biol. Chem. 257*, 14324−14332.
34. Brewer, C. B., and Peterson, J. A. (1986) *Arch. Biochem. Biophys. 249*, 515−521.
35. Li, X. Y., and Spiro, T. G. (1988) *J. Am. Chem. Soc. 110*, 6024−6033.
36. Lipscomb, J. D. (1980) *Biochemistry 19*, 3590−3599.
37. Makino, R., Iizuka, T., Ishimura, Y., Uno, T., Nishimura, Y., and Tsuboi, M. (1984) Proceedings of the Ninth International Conference on Raman Spectroscopy, The Chemical Society of Japan, Tokyo.
38. Shiro, Y., Iizuka, T., Makino, R., Ishimura, Y., and Morishima, I. (1989) *J. Am. Chem. Soc. 111*, 7707−7711.
39. Unno, M., Christian, J. F., Benson, D. E., Gerber, N. C., Sligar, S. G., and Champion, P. M. (1997) *J. Am. Chem. Soc. 119*, 6614−6620.
40. Mouro, C., Bondon, A., Jung, C., Hui Bon Hoa, G., De Certaines, J. D., Spencer, R. G., and Simonneaux, G. (1999) *FEBS Lett. 455*, 302−306.
41. Sjodin, T., Christian, J. F., Macdonald, I. D., Davydov, R., Unno, M., Sligar, S. G., Hoffman, B. M., and Champion, P. M. (2001) *Biochemistry 40*, 6852−6859.
42. Unno, M., Christian, J. F., Sjodin, T., Benson, D. E., Macdonald, I. D., Sligar, S. G., and Champion, P. M. (2002) *J. Biol. Chem. 277*, 2547−2553.
43. Tsibris, J. C. M., Tsai, R. L., Gunsalus, I. C., Orme-Johnson, W. H., Hansen, R. E., and Beinert, H. (1968) *Proc. Natl. Acad. Sci. U.S.A. 59*, 959−965.
44. Shimada, H., Nagano, S., Hori, H., and Ishimura, Y. (2001) *J. Inorg. Biochem. 83*, 255−260.
45. Hishiki, T., Shimada, H., Nagano, S., Egawa, T., Kanamori, Y., Makino, R., Park, S.-Y., Adachi, S., Shiro, Y., and Ishimura, Y. (2000) *J. Biochem. (Tokyo) 128*, 965−974.
46. Imai, M., Shimada, H., Watanabe, Y., Matsushima-Hibiya, Y., Makino, R., Koga, H., Horiuchi, T., and Ishimura, Y. (1989) *Proc. Natl. Acad. Sci. U.S.A. 86*, 7823−7827.
47. Martinis, S. A., Atkins, W. M., Stayton, P. S., and Sligar, S. G. (1989) *J. Am. Chem. Soc. 111*, 9252−9253.
48. Taniguchi, V. T., Sailasuta-Scott, N., Anson, F. C., and Gray, H. B. (1980) *Pure Appl. Chem. 52*, 2275−2281.
49. Mei, H., Wang, K., McKee, S., Wang, X., Waldner, J. L., Pielak, G. J., Durham, B., and Millett, F. (1996) *Biochemistry 35*, 15800−15806.
50. Hiraga, K., and Yutani, K. (1997) *J. Biol. Chem. 272*, 4935−4940.
51. Marcus, R. A., and Sutin, N. (1985) *Biochim. Biophys. Acta 811*, 265−322.
52. Page, C. C., Moser, C. C., Chen, X., and Dutton, P. L. (1999) *Nature 402*, 47−52.
53. Moser, C. C., Keske, J. M., Warncke, K., Farid, R. S., and Dutton, P. L. (1992) *Nature 355*, 796−802.
54. McLendon, G., and Hake, R. (1992) *Chem. Rev. 92*, 481−490.
55. Wang, K., Mei, H., Geren, L., Miller, M. A., Saunders, A., Wang, X., Waldner, J. L., Pielak, G. J., Durham, B., and Millett, F. (1996) *Biochemistry 35*, 15107−15119.
56. Brooks, H. B., and Davidson, V. L. (1994) *Biochemistry 33*, 5696−5701.
57. Tanaka, M., Ishimori, K., and Morishima, I. (1999) *Biochemistry 38*, 10463−10473.
58. Ueno, T., Kousumi, Y., Yoshizawa-Kumagaye, K., Nakajima, K., Ueyama, N., Okamura, T., and Nakamura, A. (1998) *J. Am. Chem. Soc. 120*, 12264−12273.
59. Fersht, A. R., Shi, J. P., Knill-Jones, J., Lowe, D. M., Wilkinson, A. J., Blow, D. M., Brick, P., Carter, P., Waye, M. M., and Winter, G. (1985) *Nature 314*, 235−238.
60. Bertrand, P., Mbarki, O., Asso, M., Blachard, L., Guerlesquin, F., and Tegoni, M. (1995) *Biochemistry 34*, 11071−11079.
61. Battistuzzi, G., Borsari, M., Loschi, L., Menziani, M. C., De RienZo, F., and Sola, M. (2001) *Biochemistry 40*, 6422−6430.
62. Battistuzzi, G., Borsari, M., Canters, G. W., De Waal, E., Loschi, L., Warmerdam, G., and Sola, M. (2001) *Biochemistry 40*, 6707−6712.
63. Bereton, P. S., Verhagen, M. F. J. M., Zhou, Z. H., and Adams, M. W. W. (1998) *Biochemistry 37*, 7351−7362.
64. Soriano, A., Li, D., Bian, S., Agarwal, A., and Cowan, J. A. (1996) *Biochemistry 35*, 12479−12486.
65. Nar, H., Messerschmidt, A., Huber, R., van de Kamp, M., and Canters, G. W. (1991) *J. Mol. Biol. 218*, 427−447.
66. Dangi, B., Blankman, J. I., Miller, C. J., Volkman, B. F., and Guiles, R. D. (1998) *J. Phys. Chem. B 102*, 8201−8208.

BI0261037